Journal of Alloys and Compounds 500 (2010) 161–166

Contents lists available at ScienceDirect

Journal of Alloys and Compounds

journal homepage: www.elsevier.com/locate/jallcom

Phases and phase equilibria in cobalt-rich Pr–Co–In alloys for permanent magnets

A.M. Gabay*, G.C. Hadjipanayis

Department of Physics and Astronomy, University of Delaware, Newark, DE 19716, USA

ARTICLE INFO

Article history:
Received 9 March 2010
Accepted 31 March 2010
Available online 7 April 2010

Keywords:
Rare earth alloys and compounds
Phase diagrams
Metallography
Crystal structure
Magnetic measurements
Permanent magnets

ABSTRACT

The Pr–Co–In phase equilibria related to the indium-added $PrCo_5$ permanent magnets have been systematically studied. The 800 °C isotherm and the $PrCo_5$–$PrCo_2In$ polythermal section reveal several compounds never reported for this system. One of them, the orthorhombic $Pr_3Co_9In_2$, forms peritectically at 957 °C and it is believed to be responsible for the increased coercivity of Pr–Co–In sintered magnets subjected to a post-sintering annealing. The $Pr_3Co_9In_2$ compound forms a two-phase equilibrium with $PrCo_5$; it is paramagnetic at room temperature and exhibits an antiferromagnetic ordering at 198 K. Also observed were the hexagonal $PrIn_2$ compound possibly stabilized by a small amount of cobalt and an unidentified ternary phase with the approximate composition $Pr_{45}Co_{15}In_{40}$. The work provides recommendations for the development and improvement of $PrCo_5$ permanent magnets via indium additions.

1. Introduction

In a series of recent works [1,2], we reported the strong effect of small indium additions on such well known and thoroughly studied permanent magnet materials as $Sm_2(Co, Fe, Mn)_{17}$ and $PrCo_5$. The dramatic lowering of the sintering temperature, the high values of coercivity which could be reached without sacrificing the magnet density and the perplexing inversion of the texture developed through hot plastic deformation have been tentatively associated with the indium-rich grain-boundary phases. However, these phases, which are present in small quantities and possibly under non-equilibrium conditions, could not be systematically characterized while studying permanent magnets. At the same time, according to Kalychak et al. [3,4], the current knowledge of the rare earth–cobalt–indium systems is generally limited to the structures of ternary compounds without systematic data on the phase equilibria. In the Pr–Co–In system, four such ternary compounds – $PrCoIn_5$, Pr_2CoIn_8, $Pr_{12}Co_6In$ and $PrCo_2In$ – had been discovered. Because the latter composition is the closest to that of the $PrCo_5$ compound, it may seem natural to associate the grain-boundary phase in the indium-added $PrCo_5$ sintered magnets with the $PrCo_2In$ phase. However, though the transmission electron microscopy study performed on the sintered magnets [5] did reveal the $PrCo_2In$ phase, it linked the highest coercivity values to other grain-boundary phase having a structure related to that of the $Sm_2Co_9In_3$ compound and not reported earlier for the Pr–Co–In system.

A systematic study of the phase equilibria in the cobalt-rich Pr–Co–In alloys presented in this paper is intended to shed light on the metallurgy of the $PrCo_5$-based hard magnetic alloys. The isothermal phase equilibria were established at the temperature of 800 °C, which is lower than the temperatures of the major transformation observed in the Pr–Co–In sintered magnets [2] (those transformations were additionally studied for a selected polythermal section). It must be noted in this respect that we found the $PrCo_5$ binary compound to be fairly stable at 800 °C, which is contrary to the report by Chuang et al. [6], but well in agreement with a report by Buschow [7].

2. Experimental

The Pr–Co–In alloy samples were prepared from praseodymium (purity 99.9%), cobalt (99.8%) and indium (99.9%) by arc-melting under argon. The ingots were remelted four times to ensure their homogeneity. The weight loss detected after the arc-melting varied greatly with the alloy compositions (with some ternary alloys showing no weight loss at all), which can only be explained by the varied volatility of indium. In those cases when the weight changes were significant, we corrected the nominal alloy compositions for the (assumed) indium losses. The as-prepared ingots were wrapped in tantalum foil, sealed in quartz tubes and isothermally annealed at temperatures ranging from 800 to 1100 °C. Duration of the annealing depended on the temperature as follows: 4–6 weeks at 800 °C, 2 weeks at a temperature just below the solidus temperature, 5–7 h at a temperature just above the solidus, and 1 h at 1100 °C. All annealed samples were quenched in water. Most of the cobalt-rich Pr–Co–In alloys appeared stable to air-storage at the room temperature (*i.e.*, retained their silver luster for several months); however those containing considerable amounts of the Pr–In binary phases oxidized noticeably after a few days (the high susceptibility of the Pr–In phases to oxidation was earlier observed by Delfino et al. [8]).

Microstructure of the annealed alloys was characterized using scanning electron microscopy (SEM) and energy dispersive spectrometry (EDS). SEM was performed on polished, non-etched ingot sections with a JEOL JSM-6335F instrument operating in a backscattered electron (BSE) mode. The simultaneous EDS characterization was

* Corresponding author.
E-mail address: gabay@physics.udel.edu (A.M. Gabay).

0925-8388/$ – see front matter © 2010 Elsevier B.V. All rights reserved.
doi:10.1016/j.jallcom.2010.03.247

done with an IXRF Systems instrument and software. Besides SEM–EDS, differential thermal analysis (DTA) of the alloys was performed with a PerkinElmer Pyris Diamond TG/DTA instrument. Powder X-ray diffraction (XRD) data were collected with the Cu-Kα radiation and subsequently analyzed with a Powder Cell program [9]. Magnetic properties of selected alloys were measured with a Quantum Design Magnetic Properties Measurement System.

3. Results

3.1. Phase equilibria in Co-rich Pr–Co–In alloys at 800 °C

Fig. 1 presents the phase relations determined after equilibration of the Pr–Co–In alloys for up to 6 weeks. The two-phase equilibria which we consider established are drawn as solid, whereas the dash lines represent our best judgment when the results were not fully conclusive: either too few alloys had been studied in the corresponding region or the SEM–EDS characterization detected more than three phases. The alloys situated on the right side from the $PrCo_3$ – D line (not all of them fall in to the area shown) were partially or completely molten at 800 °C.

In a good agreement with earlier studies [4], the solubility of indium in the binary Pr_2Co_{17}, $PrCo_5$, Pr_5Co_{19}, Pr_2Co_7 and $PrCo_3$ phases was found to be very low. At 800 °C, the $PrCo_2In$ phase forms two-phase equilibria with the Co and Pr_2Co_{17} phases. Fig. 2(a) shows a microstructure of the $Pr_{15.1}Co_{75.6}In_{9.3}$ alloy situated near the Pr_2Co_{17}–$PrCo_2In$ tie line (alloy 1). The amount of the Co phase in this alloy is small, but, importantly, this phase is always embedded in the Pr_2Co_{17} phase. Such morphology may suggest that Co dendrites were the first to solidify, whereas the Pr_2Co_{17} phase was later formed peritectically (there were conflicting reports of congruent melting and peritectic formation of the Pr_2Co_{17} phase in the binary Pr–Co system [10]).

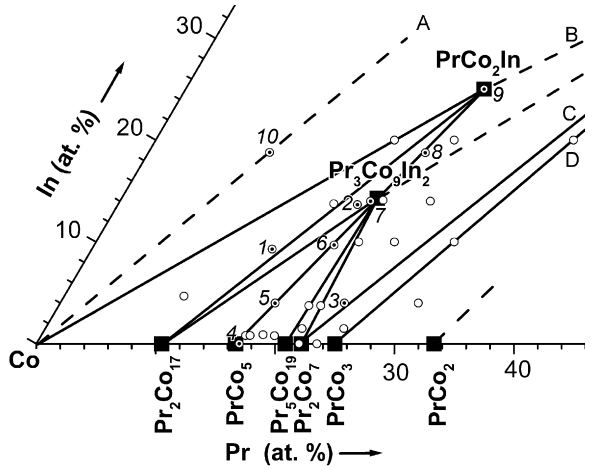

Fig. 1. The 800 °C isothermal section through Co-rich part of Pr–Co–In system. Squares represent compounds, circles indicate experimental alloys; numbered alloys are discussed in more detail in the text.

According to our findings, the $PrCo_2In$ phase does not form a two-phase equilibrium with the $PrCo_5$ phase at 800 °C. Fig. 2(b) presents microstructure of the $Pr_{20.1}Co_{66.3}In_{13.6}$ alloy which is sit-

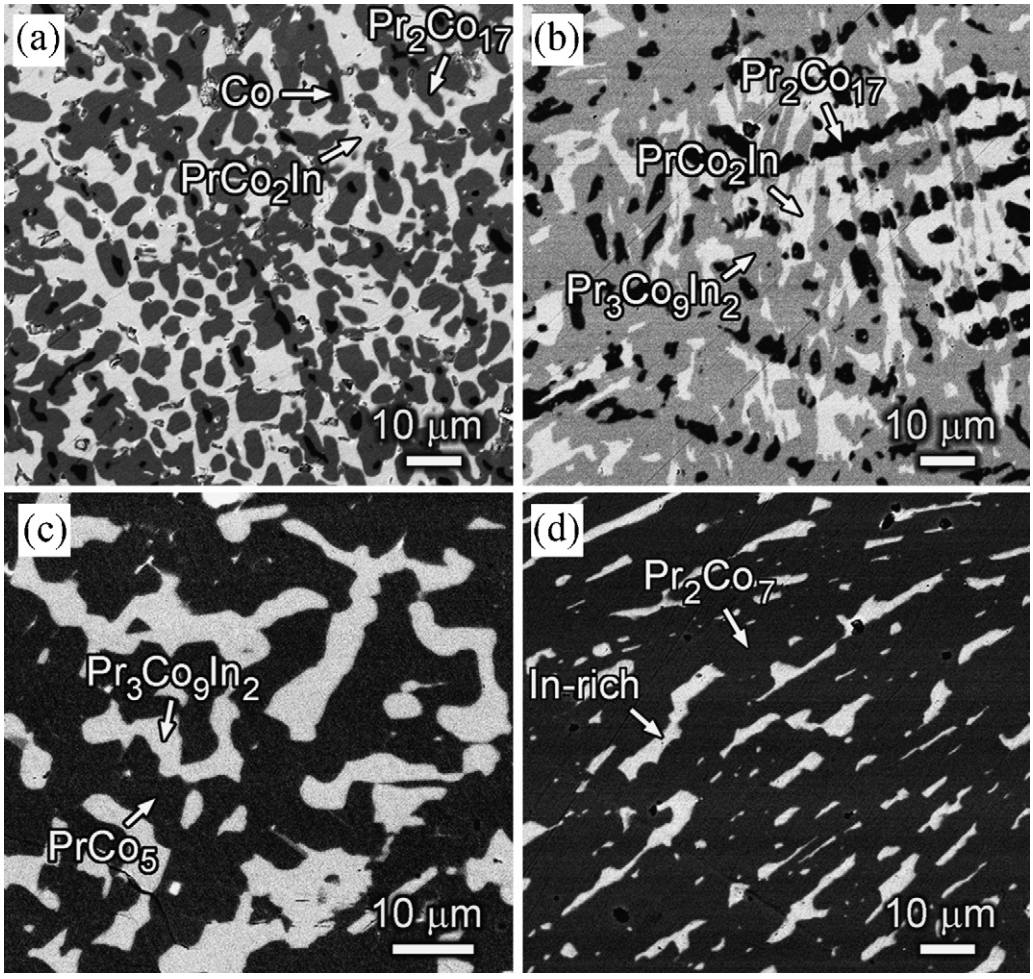

Fig. 2. BSE micrographs of (a) alloy 1 – $Pr_{15.1}Co_{75.6}In_{9.3}$, (b) alloy 2 – $Pr_{20.1}Co_{66.3}In_{13.6}$, (c) alloy 5 – $Pr_{18}Co_{78}In_4$ and (d) alloy 3 – $Pr_{23.8}Co_{72.2}In_4$ homogenized at 800 °C.

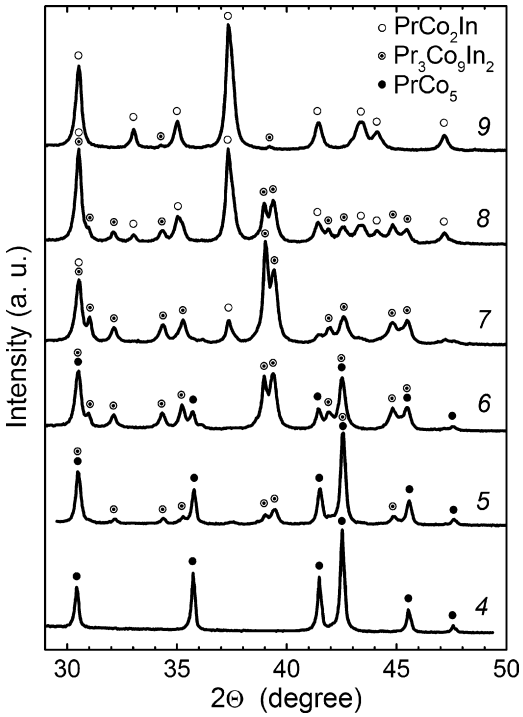

Fig. 3. Powder XRD patterns of the alloys situated along the $PrCo_5$–$Pr_3Co_9In_2$–$PrCo_2In$ line and homogenized at 800 °C: 4 – $Pr_{16.7}Co_{83.3}$, 5 – $Pr_{18}Co_{78}In_4$, 6 – $Pr_{20}Co_{70.2}In_{9.8}$, 7 – $Pr_{21}Co_{65}In_{14}$, 8 – $Pr_{23.2}Co_{58}In_{18.8}$, 9 – $Pr_{25}Co_{50}In_{25}$.

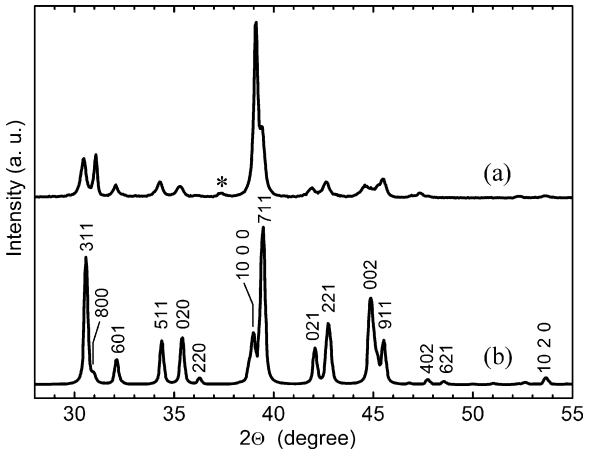

Fig. 4. (a) Powder XRD pattern of $Pr_3Co_9In_2$ alloy homogenized at 950 °C and (b) calculated pattern of hypothetical $Pr_3Co_9In_2$ structure based on the $Sm_2Co_9In_3$ type. The "*" peak belongs to the $PrCo_2In$ impurity phase.

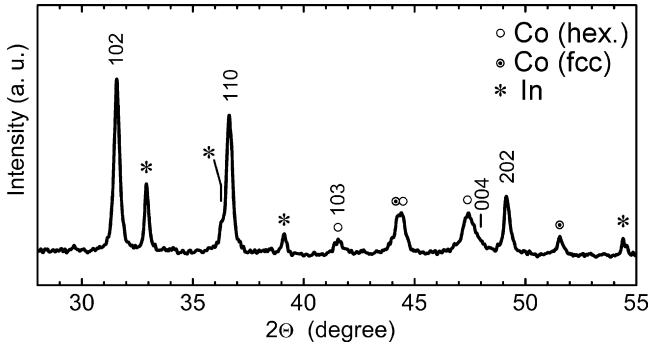

Fig. 5. Powder XRD pattern of alloy 10 ($Pr_{10.1}Co_{71.1}In_{18.8}$). Indexed are peaks of supposed $PrIn_2$ structure.

uated near the would-be $PrCo_5$–$PrCo_2In$ tie line (alloy 2). The microstructure studies feature the Pr_2Co_{17} phase (black areas; this time, the phase seems to solidify via primary dendrites), the $PrCo_2In$ phase (bright areas) and a new phase (grey areas), which we call $Pr_3Co_9In_2$. It is the $Pr_3Co_9In_2$ phase that was found to form the two-phase equilibrium with the $PrCo_5$ phase. Fig. 2(c) shows one example of the $PrCo_5 + Pr_3Co_9In_2$ microstructure observed in the alloy 5 ($Pr_{18}Co_{78}In_4$) situated on the $PrCo_5$–$Pr_3Co_9In_2$ tie line. The XRD data collected for the alloys 4–9 situated along the line connecting the $PrCo_5$ and $PrCo_2In$ compositions (and passing through the $Pr_3Co_9In_2$ composition) are shown in Fig. 3; these data are perfectly consistent with the SEM–EDS characterization. With increasing the indium content, a new XRD pattern distinct by a pair of strong peaks at 39.0° and 39.4° emerges alongside the $PrCo_5$ pattern. This new pattern becomes predominant in alloy 7 ($Pr_{21}Co_{65}In_{14}$), which is close to $Pr_3Co_9In_2$ ($Pr_{21.4}Co_{64.3}In_{14.3}$). With a further increase in the indium content, the new structure is gradually replaced by the orthorhombic $PrCo_2In$ structure (the $PrCo_2Ga$ type, $a = 0.5119$ nm, $b = 0.4089$ nm, $c = 0.7197$ nm).

Because the exact stoichiometry of the $Pr_3Co_9In_2$ compound emerged later in the study, the stoichiometic alloy was not included in the 800 °C isothermal section. Fig. 4 presents the XRD pattern of such stoichiometic alloy homogenized at 950 °C. We were able to index this pattern based on the orthorhombic $Sm_2Co_9In_3$ lattice [11] with $a = 2.3099$ nm, $b = 0.5070$ nm and $c = 0.4041$ nm. It is clear from the pattern calculated for this hypothetical structure that a further refinement is needed for the atomic positions in the new compound. Nevertheless, the match of the XRD peak positions as well as the very narrow homogeneity range observed for the new compound are strong arguments in favor of its $Pr_3Co_9In_2$ stoichiometry and its relation to the $Sm_2Co_9In_3$ structure. It should be noted that a $Pr_2Co_9In_3$ compound was neither reported in the earlier works nor found in the course of the present study.

One of the ternary phases we often observed in the cobalt-rich Pr–Co–In alloys remains unidentified. The composition of this phase determined via EDS (not a very accurate technique) is around $Pr_{45}Co_{15}In_{40}$. At 800 °C, the phase, which we call "In-rich", forms two-phase equilibria with the Pr_2Co_7 (see Fig. 2(d)) and $PrCo_3$ phases. In Fig. 1, these two-phase equilibria are represented by lines Pr_2Co_7 – C and $PrCo_3$ – D. Our attempts to obtain a pure In-rich phase or to match the corresponding XRD pattern with those of several known binary and ternary compounds (including the Lu_5NiIn_4 compound which has a similar stoichiometry) were unsuccessful.

We were not able to establish with certainty the phase equilibria in the B–$PrCo_2In$–$Pr_3Co_9In_2$–Pr_2Co_7–C region. Even after annealing for 6 weeks, the samples of different alloys featured either the $PrCo_2In + Pr_3Co_9In_2$ + In-rich microstructure (thus suggesting a $Pr_3Co_9In_2$ + In-rich two-phase equilibrium, as it is tentatively drawn in Fig. 1) or the $Pr_2Co_7 + PrCo_2In$ + In-rich phase microstructure (which would rather imply a two-phase equilibrium between the Pr_2Co_7 and $PrCo_2In$ phases).

Finally, characterization of the alloy 10 ($Pr_{10.1}Co_{71.1}In_{18.8}$) indicated the existence of yet another compound not reported for the Pr–Co–In system. The alloy exhibited a two-phase microstructure (not shown) of Co dendrites surrounded by a near-binary Pr–In phase (according to EDS this phase contains up to 4 at.% Co). The XRD spectrum of this alloy (Fig. 5) suggests that the Pr–In phase has a hexagonal structure of the $CaIn_2$ type with $a = 0.490$ nm and $c = 0.758$ nm. Though the binary compound of this structure is known to exist in the Yb–In system [12], it was not observed in the Pr–In alloys. It is possible that in alloy 10 the $PrIn_2$ compound had been stabilized by the small amount of cobalt. Note, that the XRD spectrum shown in Fig. 5 also contains the pattern of the pure indium. We believe the indium metal is a product of rapid oxidation

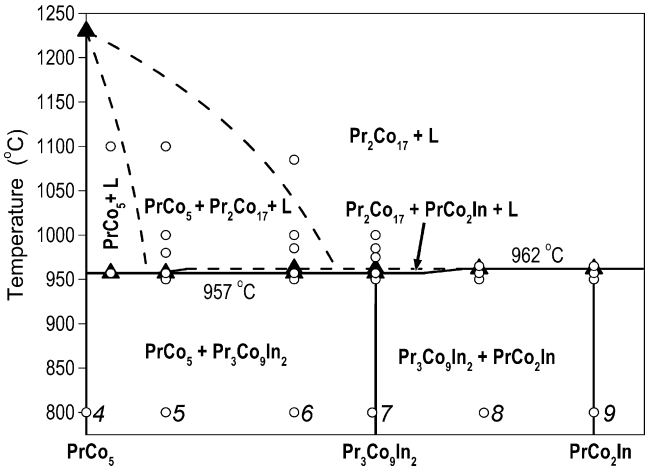

Fig. 6. Part of $PrCo_5$–$Pr_3Co_9In_2$–$PrCo_2In$ polythermal section.

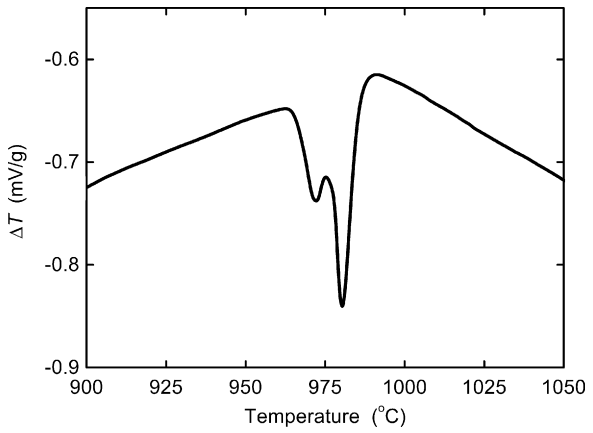

Fig. 7. Part of DTA heating curve of alloy 6 ($Pr_{20.1}Co_{70.2}In_{9.7}$) homogenized at 800 °C. Heating rate is 10 °C/min.

of the $PrIn_2$ phase in the *powdered* XRD sample. The same sample re-measured after 6 months of storing in a low vacuum exhibited a markedly greater amount of the In phase, whereas the phase we claim to be $PrIn_2$ had completely disappeared.

3.2. $PrCo_5$–$Pr_3Co_9In_2$–$PrCo_2In$ polythermal section

Our earlier studies of the indium-added $PrCo_5$ permanent magnet materials [2] identified the temperature range between 850 and 975 °C as the one of particular interest. Within this range, the heating DTA curves of the Pr–Co–In ternary alloys or those of the sintered magnets typically detected two endothermic transformations (it is important to have in mind that the sintered magnets are not exactly ternary systems; they always contain certain amount of oxygen).

In the present work, we choose ternary alloys situated on the $PrCo_5$–$Pr_3Co_9In_2$–$PrCo_2In$ line for the detailed polythermal study; its results are presented in Fig. 6. The transformation temperatures plotted as solid triangles were determined by DTA. The two melting transformations,

$$Pr_3Co_9In_2 \rightarrow Pr_2Co_{17} + PrCo_2In + L \quad (1)$$

and

$$PrCo_2In \rightarrow Pr_2Co_{17} + L, \quad (2)$$

were found to be only a few degrees apart (see Fig. 7 as an example); and it was difficult to determine accurately the highest of the two transformation temperature from the DTA data, even when the heating rate was as low as 2.5 °C/min. Moreover, when heated above the solidus temperature, the DTA results appeared to be rather controversial (even more so when cooled from above the solidus temperature). These inconsistencies might be caused by oxidation, since the argon flow used during the measurements could only partially protect the highly reactive samples. Therefore, the high-temperature part of the polythermal section had to be reconstructed based on the SEM–EDS characterization of the annealed and quenched samples represented by the open circles in Fig. 6. According to this reconstruction, the high-temperature stability of the $PrCo_5$ phase in the equilibrium with the ternary liquid decreases sharply as the indium content in the liquid increases.

The as-prepared $Pr_3Co_9In_2$ alloy exhibited a non-equilibrium microstructure (not shown) of the Pr_2Co_{17} dendrites and three ternary phases, $Pr_3Co_9In_2$, $PrCo_2In$ and "In-rich" one. Fig. 8(a) shows the microstructure of the same alloy after homogenization for 2 weeks at 950 °C, when it becomes nearly a single phase. The *subsequent* exposure to 957 °C (a transformation temperature suggested by the DTA results) produces large Pr_2Co_{17} precipitates surrounded by a mixture of the $PrCo_2In$ and In-rich phases, but most of the $Pr_3Co_9In_2$ phase remains intact. This apparent four-phase equilibrium confirms that 957 °C is the temperature of a peritecic reaction (1). The temperature of peritectic reaction (2), 962 °C, has been determined in a similar fashion.

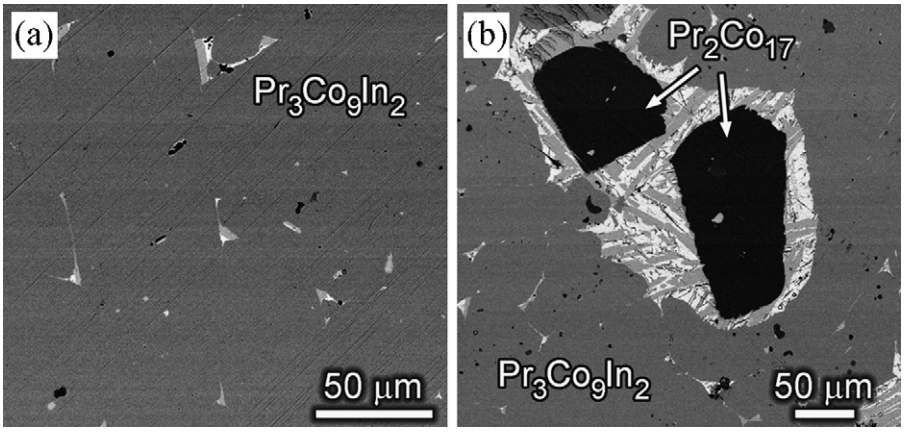

Fig. 8. BSE micrographs of $Pr_3Co_9In_2$ alloy (a) homogenized for 2 weeks at 950 °C and (b) subsequently annealed for 7 h at 957 °C.

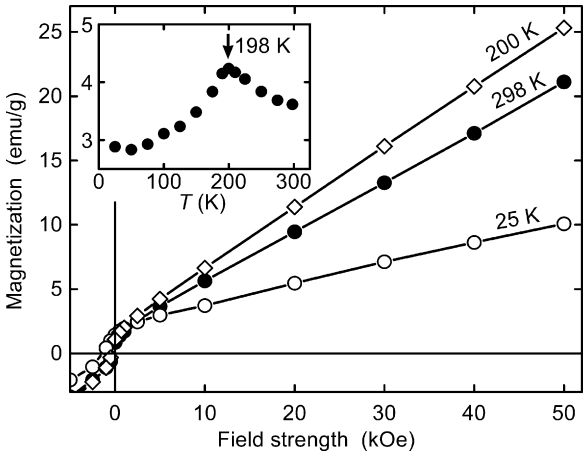

Fig. 9. Magnetization curves of $Pr_3Co_9In_2$ alloy homogenized at 950 °C. Inset presents magnetization values at 5 kOe as a function of temperature.

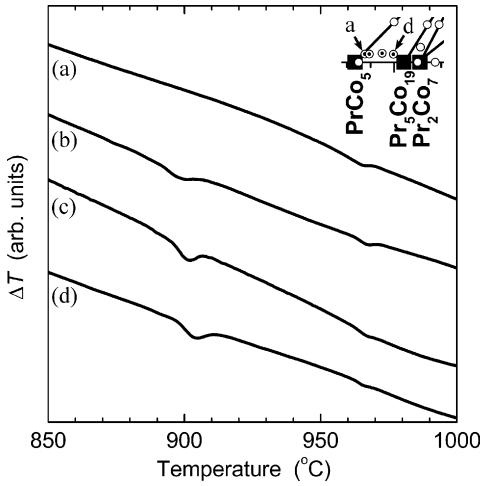

Fig. 10. Parts of 10 °C/min DTA heating curves of (a) $Pr_{17.1}Co_{82}In_{0.9}$, (b) $Pr_{17.5}Co_{81.6}In_{0.9}$, (c) $Pr_{18.5}Co_{80.5}In_1$ and (d) $Pr_{19.5}Co_{79.6}In_{0.9}$ alloys homogenized at 800 °C. Inset shows the alloy compositions in the 800 °C isothermal section.

3.3. Magnetic properties of $Pr_3Co_9In_2$ phase

Fig. 9 presents magnetization curves of the nearly single phase $Pr_3Co_9In_2$ alloy. Apart from the small amount of a ferromagnetic impurity phase (probably, $PrCo_5$), which is evident from the low-field data, the curves exhibit a paramagnetic behavior. At room temperature, the susceptibility of the paramagnetic phase is 3.8×10^{-4} emu/g Oe. The magnetization measured at the constant field of 5 kOe (at this field the magnetization of the ferromagnetic impurity phase is saturated) exhibits a sharp maximum at 198 K, thus indicating the apparent transition from paramagnetic to antiferromagnetic state.

4. Discussion

The situation when the Sm–Co–In and Pr–Co–In, the two systems one might reasonably expect to be quite similar, feature so compositionally different yet structurally related compounds as $Sm_2Co_9In_3$ [4,11] and $Pr_3Co_9In_2$ seems peculiar and even somewhat unsettling. In view of the finding presented in this paper, one may even consider a re-investigation of the Sm–Co–In system (unfortunately, we were not able to access the original report on the $Sm_2Co_9In_3$ compound). On the other hand, the stoichiometry of the $Pr_3Co_9In_2$ compound which we report and which is situated exactly between the $PrCo_5$ and $PrCo_2In$ compounds appears to be rather reasonable, since the structure of this compound (if it is indeed of the $Sm_2Co_9In_3$ type) incorporates elements of both the $PrCo_5$ and $PrCo_2In$ structures [3,4].

If our reconstruction of the polythermal phase equilibria is correct, the need for a prolonged homogenization for obtaining the $Pr_3Co_9In_2$ compound is caused not only by the peritectic mechanism of its formation, but also by the prior formation of the $PrCo_2In$ compound, which is closer to the composition of the liquid phase. The same thing must apply to the Pr–Co–In sintered magnets [2,5]; once the magnets with as little as 0.5–1.5 at.% In are cooled from the sintering temperature of 975 °C (*i.e.*, from the $PrCo_5$ + L phase region), they contain the *metastable* $PrCo_2In$ phase. The function of post-sintering annealing is to produce the stable $Pr_3Co_9In_2$ phase, which tends to envelop the $PrCo_5$ grains [5] insulating them magnetically and, therefore, contributing to the coercivity increase (the short duration of the post-sintering annealing compared to the homogenization of ingots can be explained by the much finer microstructure of the sintered magnets). We found [2] that the optimum annealing temperature sharply decreases with the Pr content. Because of the partial oxidation, the nominal composition of the sintered magnets cannot be directly compared to the Pr–Co–In phase diagram, but the latter does exhibit a similarly sharp decline of the solidus temperature at similarly low indium concentrations. The DTA curves of four alloys containing 0.9–1 at.% In shown in Fig. 10 demonstrate that within the $PrCo_5$–$Pr_3Co_9In_2$–Pr_5Co_{19} triangle, the solidus temperature is more than 50 °C lower than at the $PrCo_5$–$Pr_3Co_9In_2$ tie line.

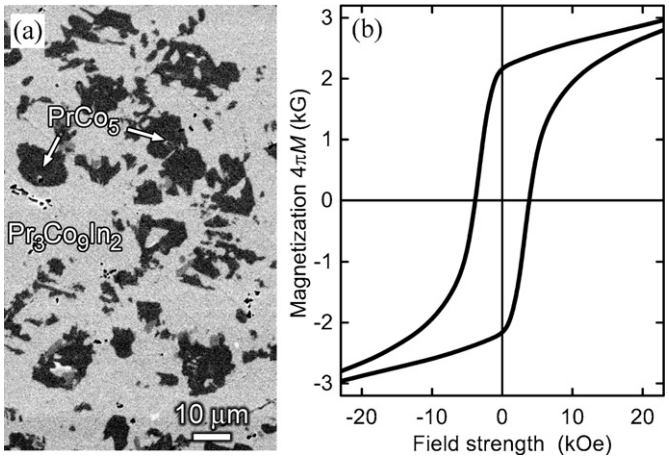

Fig. 11. (a) BSE micrograph and (b) room-temperature hysteresis loop of alloy 6 ($Pr_{20}Co_{70.2}In_{9.8}$) homogenized for 4 weeks at 800 °C. Maximum applied field is 50 kOe; data are corrected for self-demagnetizing field.

It is interesting to note that since the equilibrium room-temperature microstructure of the alloys situated on the $PrCo_5$–$Pr_3Co_9In_2$ tie line contain a highly anisotropic ferromagnetic phase and a paramagnetic phase, magnetic hardness may be expected in these alloys even without the use of a powder metallurgy. Fig. 11(a) shows the equilibrium microstructure of alloy 6 ($Pr_{20}Co_{70.2}In_{9.8}$) featuring small (smaller than 15 μm) areas of the $PrCo_5$ phase embedded into the paramagnetic $Pr_3Co_9In_2$ matrix. The bulk alloy exhibited a moderate coercivity of 3.8 kOe; judging from this result, it is probably possible to develop "cast and annealed" permanent magnets with the $PrCo_5$ + $Pr_3Co_9In_2$ microstructure. However, the low saturation magnetization of such magnets and the high cost associated of the large indium additions make them unlikely candidates for practical applications.

5. Conclusion

The work presents a detailed, though far from complete, characterization of the phase equilibria in the cobalt-rich Pr–Co–In alloys and provides guidelines for development and improvement of $PrCo_5$ permanent magnets via indium additions. In order to avoid undesirable ferromagnetic phases and assure magnetic insulation of the $PrCo_5$ grains, the optimum *effective* magnet composition should be situated on the $PrCo_5 + Pr_3Co_9In_2$ tie line. Heat treatment of the magnet must favor formation of the $Pr_3Co_9In_2$ phase, which is stable below 957 °C.

Acknowledgement

This work was supported by ONR through contract N00014-09-1-0606.

References

[1] A.M. Gabay, M. Marinescu, J.F. Liu, G.C. Hadjipanayis, IEEE Trans. Magn. 44 (2008) 4218–4221.
[2] A.M. Gabay, M. Marinescu, J.F. Liu, G.C. Hadjipanayis, IEEE Trans. Magn. 45 (2009) 4409–4412.
[3] Ya.M. Kalychak, J. Alloys Compd. 291 (1999) 80–88.
[4] Ya.M. Kalychak, V.I. Zaremba, R. Pöttgen, M. Lukachuk, R.-D. Hoffmann, Rare earth-transition metal – indides, in: K.A. Gschneider Jr., V.K. Pecharsky, J.-C. Bünzli (Eds.), Handbook on the Physics and Chemistry of Rare Earths, vol. 34, Elsevier, Amsterdam, 2005, pp. 1–133 (Chapter 218).
[5] W.F. Li, A.M. Gabay, C. Ni, G.C. Hadjipanayis, J. Appl. Phys. 107 (2010) 063307.
[6] Y.C. Chuang, C.H. Wu, S.C. Chang, T.C. Li, Y.C. Wang, J. Less-Common Met. 125 (1986) 25–32.
[7] K.H.J. Buschow, J. Less-Common Met. 37 (1974) 91–101.
[8] S. Delfino, A. Saccone, R. Ferro, J. Less-Common Met. 65 (1979) 181–190.
[9] W. Kraus, G. Nolze, J. Appl. Crystallogr. 29 (1996) 301–303.
[10] C.H. Wu, Y.C. Chuang, X.M. Jin, X.H. Guan, Z. Metallkd 83 (1992) 32–34.
[11] P. Villars (Ed.), Pearson's Handbook, Crystallographic Data for Intermetallic Phases (desk ed.), ASM, Materials Park, OH, 1997.
[12] O.D. McMasters, C.L. Nipper, K.A. Gschneidner, J. Less-Common Met. 23 (1971) 253–262.